Chem Soc Rev

Cite this: *Chem. Soc. Rev.*, 2011, **40**, 5457–5471

www.rsc.org/csr

CRITICAL REVIEW

Ordered patterns and structures *via* interfacial self-assembly: superlattices, honeycomb structures and coffee rings

Hongmin Ma and Jingcheng Hao*

Received 4th March 2011
DOI: 10.1039/c1cs15059f

Self-assembly is now being intensively studied in chemistry, physics, biology, and materials engineering and has become an important "bottom-up" approach to create intriguing structures for different applications. Self-assembly is not only a practical approach for creating a variety of nanostructures, but also shows great superiority in building hierarchical structures with orders on different length scales. The early work in self-assembly focused on molecular self-assembly in bulk solution, including the resultant dye aggregates, liposomes, vesicles, liquid crystals, gels and so on. Interfacial self-assembly has been a great concern over the last two decades, largely because of the unique and ingenious roles of this method for constructing materials at interfaces, such as self-assembled monolayers, Langmuir–Blodgett films, and capsules. Nanocrystal superlattices, honeycomb films and coffee rings are intriguing structural materials with more complex features and can be prepared by interfacial self-assembly on different length scales. In this *critical review*, we outline the recent development in the preparation and application of colloidal nanocrystal superlattices, honeycomb-patterned macroporous structures by the breath figure method, and coffee-ring-like patterns (247 references).

1. Introduction

With the development of supramolecular chemistry and the rise of nanotechnology, chemical self-assembly has become an important "bottom-up" approach to create intriguing materials of nano- and micro-structures.[1–6] These self-assembled structural materials have shown great potential for application in many fields, including microelectronics,[7–9] medicine and biotechnology,[10,11] catalysis,[12,13] sensors,[14,15] solar and fuel cells,[16,17] and so on. The continuous discovery of new building blocks, such as anisotropic particles,[18] Janus particles,[19] reconfigurable colloids,[20,21] processable graphenes,[22] and

Key Laboratory of Colloid and Interface Chemistry of Ministry of Education, Shandong University, Jinan 250100, P.R. China. E-mail: jhao@sdu.edu.cn; Fax: +86-531-88564750

Hongmin Ma

Hongmin Ma received both his BS and MS in Applied Chemistry from University of Jinan in 2005 and 2008, respectively. He is currently pursuing his PhD in Colloid and Interface Chemistry with Professor Jingcheng Hao at Shandong University investigating self-assembly at all scales at surfaces.

Jingcheng Hao

Jingcheng Hao received his PhD from the Lanzhou Institute of Chemical Physics, CAS, in 1995. He is currently a Professor and the Director of the Key Laboratory of Colloid and Interface Chemistry (Shandong University), Ministry of Education. His research focuses on colloid and interfacial sciences, including surfactants in solution and self-assembly at all scales in bulk solution and at surfaces. He currently serves on the Editorial Boards of Langmuir, Advances in Colloid and Interface Sciences, Journal of Colloid and Interface Sciences, and Colloids & Surfaces A, among others, and has published over 170 articles including original research papers, reviews, books, and book chapters.

new amphiphiles,[23,24] enables us to create more complex and functional systems. However, the need for increased complexity is growing and there is still a long way for us to approach the complexity of what nature has created *via* self-assembly,[25] ranging from cell membranes to organisms. One of the top 25 big questions facing scientists today collected in the special issue of *Science* for the journal's 125th anniversary is "How far can we push chemical self-assembly".[26] Up to now, we still cannot give reasonable answers to this compelling puzzle, but we are delighted to see that considerable advances in self-assembly have been achieved over the past 5 years. A comprehensive review of self-assembly has been presented by Ariga and co-workers.[27]

Self-assembly was originally defined as a process in which molecules or parts of molecules spontaneously form ordered aggregates, usually by non-covalent interactions, that is, supramolecular self-assembly or molecular self-assembly.[28] Now it has been widely accepted that self-assembly refers to autonomous organization of various components into patterns or structures through many different kinds of interactions.[29,30] The term "self-assembly" is used increasingly in many disciplines and there is no clear-cut definition of self-assembly.[31] As a result, the term has been overused to the point of becoming a cliché.[32] And we are often confused with the difference between self-assembly and self-organization. Both self-assembly and self-organization give rise to ordered patterns or structures from a disordered precursor state without human intervention and they are often used interchangeably. Many attempts have been made to distinguish the two concepts on the bases of thermodynamics and other rules.[33] Generally self-organization implies a non-equilibrium process and self-assembly is reserved for spontaneous processes tending toward equilibrium,[33] which have been defined as dynamic self-assembly and static self-assembly, respectively, by Whitesides and Grzybowski.[32] It should be noted that each scientific discipline tends to have its own definitions of the two concepts and there are some systems that are difficult to classify as either process. Maybe a general theory combining the two concepts will be proposed one day and it is not necessary to distinguish the two processes. A general concept of self-assembly is adopted in this review.

The early works of self-assembly focus on the formation of patterns and structures on the molecular-level through non-covalent interactions, such as hydrogen bonding, coordination interactions, and hydrophobic interactions.[34–37] Besides the well studied molecular aggregates in solution, such as micelles, liposomes, vesicles, liquid crystals, and gels, various nanostructures of molecular components may also be formed at interfaces.[38,39] Here we review recent work on the preparation and application of self-assembled patterns and structures at interfaces on relatively large scales, most of which have been published in the past 5 years. The building blocks focused upon in this review are non-molecular systems, including nanocrystals, clusters, polymers, nanocomposites, and so on. Self-assembly at liquid/liquid interfaces is not included in this review and the reader is referred to the work of other groups.[40,41] Special attention will be given to evaporation-induced ordered nano- and micro-structures on solid surfaces, including colloidal nanocrystal superlattices, honeycomb-patterned macroporous structures, and coffee-ring-like patterns.

2. Colloidal nanocrystal superlattices

Colloidal nanocrystals with tailored properties can be easily prepared through exquisite control over the size, shape, composition and surface chemistry, and thus are becoming attractive and promising building blocks for advanced materials and devices.[42–45] The bottleneck to achieve such applications is the assembly of these building blocks into periodic and functional structures. Two- and three-dimensional superlattices (in thin film, powder, and solid bulk form) are a type of materials of fundamental interest and technological importance.[46,47] Nanocrystal superlattices (also called supercrystals) can form both at interfaces and in solution.[48] In keeping with the subject of this review, the formation of nanocrystal superlattices in solution is not taken into consideration here.

2.1. Preparation methods

Nanocrystal superlattices were originally prepared by depositing nanocrystal suspensions on substrates (such as carbon-coated copper grids or silicon wafers), followed by evaporating the solvents.[49,50] The relatively weak attractions between nanocrystals, which are efficiently screened in solution, become manifest as the solvent evaporates. Electrostatic interactions, van der Waals forces, steric repulsion, Coulombic forces, and dipolar interactions have been identified as the driving forces to induce the formation of superlattices. Although certain aspects of this process can be explained using thermodynamic arguments alone, it is in principle a non-equilibrium process.

Nanocrystal superlattices can also be slowly deposited on substrates which are submerged vertically or aslant in nanocrystal suspensions in a vial.[51] Similar to the drop-casting method, various conditions such as solvent, nanocrystal concentration and type of substrate can be adjusted to obtain superlattices with high qualities. Moreover, the solvent evaporation rate can be controlled through a variation of the solvent pressure, which could be achieved by placing the vial in different pressure environments.

Evaporation-induced formation of nanocrystal superlattices is a far-from-equilibrium process, thus the order of superlattices is often localized. However, applications of nanocrystal superlattices in electronic or magnetic devices require efficient methods for the fabrication of well-ordered superlattices on large areas. Bodnarchuk and co-workers reported a reel-to-reel compatible large-area coating technique for superlattice fabrication, which is given by doctor blade casting.[52] The prepared thin superlattice films exhibit hexagonally closely packed arrangements, which are formed by a top-down growth. The ordering in the topmost layer extends over large areas, although some defects and irregularities are found. Lin and co-workers proposed a simple and efficient method for fabricating large-area (>1 cm^2), three-dimensional supercrystal films.[53] In this method, Janus nanoparticle (top face solvent-phobic and bottom face solvent-philic) films with an arbitrary number of close-packed nanoparticle monolayers can be formed using layer-by-layer (LbL) assembly from suspensions of thiolate-passivated gold or silver colloids (Fig. 1).

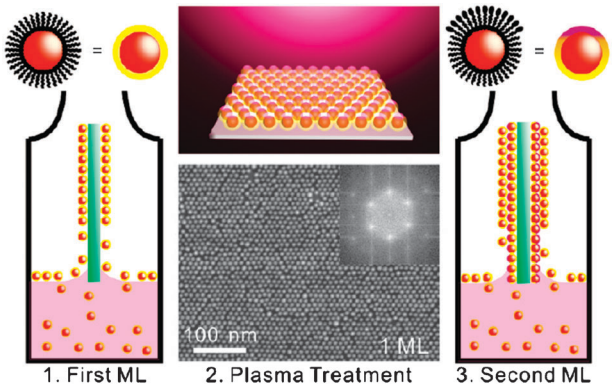

Fig. 1 Schematic illustration of the plasma-assisted LbL assembly process. The FE-SEM image obtained from the first monolayer of AuNPs after plasma treatment indicates a long-range close-packed nanoparticle superlattice. Reproduced with permission from ref. 53, copyright 2010 American Chemical Society.

While nanocrystal superlattices over large areas can be prepared through various approaches, patterning such superlattices is essential in making use of these structures. The combination of "bottom-up" self-assembly approaches with well-known "top-down" techniques seems to be effective in controlling the positioning and size of superlattices. Cheng and co-workers reported an approach for patterning superlattices that involves moulding microdroplets containing the nanoparticles and spatially regulating their dewetting process.[54] By sandwiching a nanoparticle solution between a micropatterned polydimethylsiloxane (PDMS) mould and a solid substrate, this approach can provide rational control over the local nucleation and growth of the nanoparticle superlattices, patterning nanoparticle superlattices over large areas into a number of versatile structures. Akey and co-workers reported the fabrication of large three-dimensional superlattices by controlling solvent evaporation in a lithographically defined structure in which solution is entrained into capillary channels.[55] The combination of lithographic patterning and microfluidic flow generates long-range order over the micrometre scale and controlled placement of superlattices.

2.2. Single-component superlattices

2.2.1. Formation of long-range ordered superlattices. A variety of nanocrystals with different shapes, sizes and compositions, ranging from metals and metal oxides to semiconductors, have been used as building blocks to prepare superlattice assemblies. The preparation of nanocrystals monodisperse in size and shape is prerequisite for the formation of ordered superlattices.[56] Besides the spherical nanoparticles, non-spherical (faceted) nanocrystals have also received considerable attention because they can form more abundant and complex superlattices and may offer certain enhanced characteristics with their anisotropic assemblies.[57] In addition to the monodispersity, nanocrystal size can influence the morphology of self-assembled superlattices. Rupich and co-workers reported a size-dependent multiple twinning in PbS superlattices.[58] A strong tendency to form multiply twinned face-centered cubic superlattices with decahedral and icosahedral symmetry was observed for large (>7 nm) PbS nanocrystals. On the other hand, superlattices of small (<4 nm) PbS nanocrystals exhibited no twinning. The dramatic difference in the twinning probability showed that twinning energy in a nanocrystal superlattice is strongly size dependent. In addition, the interparticle potentials acting during the self-assembly process are "softer" in the case of larger PbS nanocrystals, thus favoring the formation of multiply twinned superlattices.

As mentioned above, evaporation-induced formation of nanocrystal superlattices is a non-equilibrium process. One of the key factors in creating highly ordered superlattices is the slow and regulated evaporation rate of the solvent. It has been found that both the evaporation kinetics and the amount of excess capping ligands affect the formation of superlattices. Bigioni and co-workers performed direct, real-time and real-space observations of nanocrystal self-assembly.[59] The results showed that formation of long-range ordered superlattices was controlled by evaporation kinetics and particle interactions with the liquid–air interface. In the presence of an attractive particle–interface interaction, rapid early-stage evaporation dynamically produces a two-dimensional solution of nanoparticles at the liquid/air interface, from which nanoparticle islands nucleate and grow (Fig. 2). This self-assembly mechanism produces monolayers with exceptional long-range ordering that are compact over macroscopic areas, despite the far-from-equilibrium evaporation process. They also found that the presence of excess dodecanethiol (capping ligand) plays a key role in the interfacial island nucleation and growth. Similarly, excess dodecanethiol ligands were found to be critical for binary nanoparticle superlattice formation, highlighting the multiple roles of organic capping ligand molecules.[60]

The chemical properties and molecular configuration of capping ligands also influence the formation of superlattices. Weak interparticle interactions are important to the formation of a highly ordered array in that they prevent amorphous aggregation prior to the formation of a thermodynamically stable, close-packed structure. Nishio and co-workers prepared a highly ordered 3D superlattice assembly using fluorinated tetraethylene glycol-stabilized Au nanoparticles as building blocks.[61] However, non-fluorinated Au nanoparticles produced only amorphous aggregations under the same conditions. These results indicate that the fluorine feature on the surface of nanoparticles is critical for the superlattice formation. Wang and co-workers recently demonstrated that mutual transformation between random nanoparticles and their well-ordered superlattices could be unified by a proposed

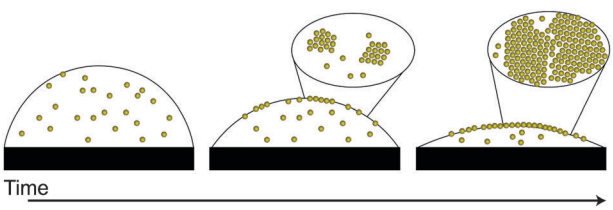

Fig. 2 Schematic diagram of the self-assembly process during the early stages of drying, showing how nanoparticles are captured by a quickly receding liquid/air interface. Reproduced with permission from ref. 59, copyright 2006 Nature Publishing Group.

model of ligand configuration.[62] When the ligand chains capped on PbSe nanoparticles were disordered at room temperature, nanoparticles existed separately in solution and thus showed random states; comparatively, the ligand chains capped on nanoparticles in an ordered state in solution would correspond to superlattice structures.

2.2.2. Superlattices with optical properties. Noble metal nanoparticles are the most well studied nanocrystals because of their size monodispersity, shape controllability, facile surface functionalization, and unique optical properties in the visible light region. The strong localized surface plasmon resonance (LSPR) of noble metal nanoparticles enables their ordered arrays as good candidates for plasmonic materials.

Gwo and co-workers have prepared highly ordered 2D and 3D superlattices of alkanethiolate-stabilized gold nanoparticles (AuNPs) with varying lattice constants, which can be controlled by the alkyl chain lengths.[53,63] It has been demonstrated that these superlattices show strong collective surface plasmon resonance extinction bands which are tunable *via* near-field coupling of adjacent nanoparticles.[63] Furthermore, the chain-length-dependent near-field coupling is both transverse (intralayer) and longitudinal (interlayer) in the multilayered (3D) superlattices.[53] The multiple longitudinal plasmonic coupling enables broadband tuning of the collective plasmon response over a wide spectral range (visible and near-IR) and opens a route to design plasmonic metamaterials.

The LSPR band of noble metal nanoparticles is sensitive to nanoparticle composition, size, shape and local dielectric environment. Tao and co-workers demonstrated the formation of both 2D and 3D superlattices of polyhedral silver nanocrystals.[64,65] Tunability of the optical response over the entire visible range can be achieved by controlling interparticle spacing, density and packing symmetry in the 2D superlattices.[64] A frequency-selective response in the visible wavelengths is observed in the 3D superlattices of silver nanocrystals.[65] Extensive long-range order mediated by exceptional colloid monodispersity gives rise to optical passbands that can be tuned by particle volume fraction. These metallic supercrystals present a new paradigm for the fabrication of plasmonic metamaterials with potential application in spectroscopic sensors, subwavelength optics and integrated devices that utilize field-enhancement effects.

2.2.3. Superlattices with mechanical properties. While optical and electronic properties of nanocrystal superlattices have been studied extensively, mechanical properties (including hardness and modulus, residual stress and strain, and fracture toughness) have received less attention. Tam and co-workers recently reported the first nanoindentation studies of well-ordered 3D superlattices of lead sulfide nanocrystals stabilized with oleic acid ligands.[66] The experimental results showed that the modulus and hardness of these supercrystals were similar to hard polymers at 1.7 GPa and 70 MPa, respectively, and the fracture toughness was 40 KPa $m^{-1/2}$. The mechanical response revealed the brittle nature of these materials.

Podsiadlo and co-workers found that the mechanical properties of nanocrystal superlattices are dominated by not only the nanocrystal size and organic capping agents, but also the degree of ordering.[67] The nature of the organic capping agents surrounding the inorganic cores significantly affects the mechanical properties while a direct relationship between the core size and hardness/modulus has been revealed. This observation suggests that the matrices of organic ligands have properties similar to polymers. The supercrystals with a high degree of ordering were found to show a more than 2-fold increase in hardness and elastic moduli due to tighter packing of the nanocrystals, and smaller interparticle distances.

2.3. Multi-component superlattices

2.3.1. Variety in binary nanocrystal superlattices. The most remarkable development in nanocrystal superlattices has been the preparation of multi-component superlattices, especially binary nanocrystal superlattices (BNSLs). Assembling two different types of nanoparticles into a BNSL not only combines the distinct properties of the individual components but offers new collective properties arising from controlled nanoparticle interactions. Motivated by the emerging concept of metamaterials, a variety of BNSLs were prepared from metallic–metallic (Me–Me), semiconductor–semiconductor (Se–Se), metallic–semiconductor (Me–Se), semiconductor–magnetic (Se–Ma), metallic–magnetic (Me–Ma), and magnetic–magnetic (Ma–Ma) nanocrystal combinations. Several different BNSL structures isostructural with intermetallic alloys, such as NaCl, AlB_2, $CaCu_5$, $NaZn_{13}$, have been prepared by tuning the size ratio and stoichiometry of two building blocks. While the icosahedral form of AB_{13} structures (*ico*-AB_{13}) has been reported as the only structure with AB_{13} stoichiometry, Shevchenko and co-workers found an unanticipated polymorph of lower packing density (*cub*-AB_{13}).[68] Nanoparticles often self-assemble into hexagonal-close-packed (hcp) and face-centered-cubic (fcc) structures. Talapin and co-workers observed the formation of non-close-packed simple-hexagonal (sh) superlattices of nearly spherical nanocrystals.[69] The richness and diversity of BNSLs enable them as a new class of multifunctional materials. The representative superlattice structures with different stoichiometry and packing symmetry prepared from various nanocrystal combinations are summarized in Table 1.

2.3.2. Driving forces for multi-component superlattices. While a variety of BNSLs can be prepared from different nanoparticle combinations, the driving forces for BNSL formation are not well understood. Before the discovery of BNSLs, binary colloidal crystals have been well studied and can be formed by crystallization of a binary mixture of micrometre-sized colloids.[85,86] In the case of superlattices of micrometre-sized colloids, unless by applying an external field[87] or by using oppositely charged particles,[88,89] the self-assembly process is generally considered to be driven only by an increase in entropy.[90] Because the formation of some BNSL structures, such as AB_2 and AB_{13}, are in accordance with the phase diagrams of binary hard-sphere mixtures, the space filling principle (maximization of the packing density) has also been proposed as the driving force for the formation of BNSLs.[82]

However, the monolayer-stabilized nanoparticles used to form BNSLs cannot be considered as simple hard spheres because various interparticle interactions (van der Waals, steric

Table 1 Summary of different superlattice structures from various nanocrystal combinations

	AB	AlB_2	$MgZn_2$	$CaCu_5$	*ico*-$NaZn_{13}$	*cub*-$NaZn_{13}$
Me–Me	Au/Ag[70]	Au/Au[71] Au/Ag[70]				
Se–Se	PbTe/Ag_2Te[72]	CdTe/CdSe[73] PbSe/CdSe[74,75]	CdTe/CdSe[73] PbSe/CdSe[75]	CdTe/CdSe[73,76]	CdTe/CdSe[73] PbSe/CdSe[75]	CdTe/CdSe[73,76] PbSe/CdSe[74]
Me–Se		CdSe/Au[77,78] PbS/Pd[79]	PbSe/Pd[79]	CdSe/Au[78] PbSe/Au[79]	PbS/Au[77] CdSe/Au[77] PbSe/Pd[68] PbSe/Ag[79]	CdSe/Au[78] PbSe/Pd[68,79]
Ma–Ma		Fe_3O_4/Fe_3O_4[80]		$CoPt_3/CoPt_3$[81]	Fe_3O_4/Fe_3O_4[80]	Fe_3O_4/Fe_3O_4[80]
Se–Ma		PbSe/Fe_2O_3[82]		PbSe/Fe_2O_3[82]	PbSe/Fe_2O_3[82]	
Me–Ma	Fe/Au[83] Fe_2O_3/Au[79]	Fe_2O_3/Au[84]				

and dipolar forces) cannot be ignored in the nanoscale. And indeed, the very rich phase diagrams of BNSLs go far beyond the predictions of hard sphere models which only take into account the entropy potential.[51,68,69,79,91] It is now well accepted that the diversity of BNSL structures is a result of the subtle balance between various possible driving forces, including entropy, Coulomb interactions, van der Waals forces, charge–dipole, dipole–dipole, and ligand–ligand interactions.[51,92]

The contributions of each of these driving forces vary for different nanoparticle combinations. Shevchenko and co-workers demonstrated that electrical charges on organically stabilized nanoparticles determine the stoichiometry and other contributions from entropic, van der Waals, steric and dipolar forces stabilize the variety of BNSL structures.[79] Electrostatic effects even can induce the formation of non-close-packed structures, diamond-like lattice.[91] By varying the nanocrystal size ratio, entropy increases were demonstrated as the dominant driving force for the formation of semiconductor BNSLs.[73,75] In contrast to semiconductor combinations, when metal nanocrystals are involved, the van der Waals attractions become important.[75,92] Although the dominant driving force can be revealed through systematic investigation of the influencing parameters independently,[73] general principles combining both energetic and entropic contributions for the formation of BNSLs are still challenged.

2.3.3. Collective properties of BNSLs. The wide interests and great efforts for the preparation of BNSLs are motivated by the new collective properties arising from the interactions of different nanoparticles. Several examples concerning the synergistic effects of different nanoparticles in hybrid assemblies have been reported. Kagan and co-workers demonstrated the electronic energy transfer between CdSe nanoparticles of different size which formed close packed quantum dot solids.[93] Enhancement of the luminescence of the large nanoparticles accompanied by quenching of the luminescence of the small nanoparticles was observed. This observation is caused by long-range resonance transfer of electronic excitations from the more electronically confined states of the small nanoparticles to the higher excited states of the large nanoparticles. Zeng and co-workers reported the fabrication of binary assemblies of FePt and Fe_3O_4 nanoparticles, which can be converted into FePt-Fe_3Pt nanocomposites.[94] Enhanced energy density is obtained due to magnetic exchange coupling, where FePt is a magnetically hard phase and Fe_3Pt is a soft phase.

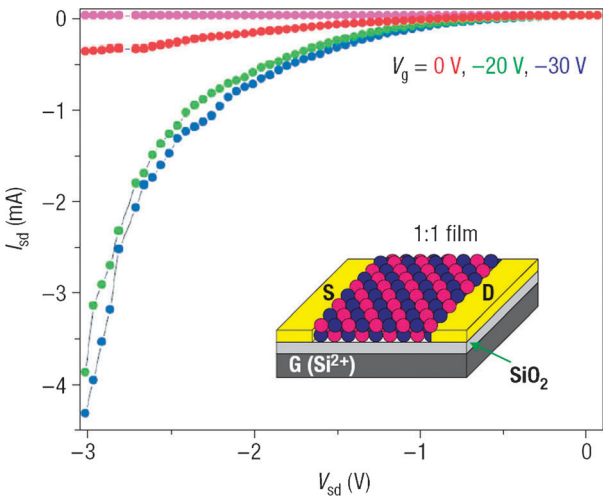

Fig. 3 Electronic measurements of 1 : 1 PbTe-Ag_2Te binary nanocrystal film demonstrating high p-type conductivity and no gate response. Reproduced with permission from ref. 72, copyright 2007 Nature Publishing Group.

In contrast to these random mixtures and glassy solids of nanoparticles, nanocrystal superlattices can provide precise stoichiometry, uniformity of packing, and rigorous control of the interparticle distance. More striking collective properties are expected for BNSLs. Urban and co-workers have reported the strong enhancement of p-type conductivity of AB-type PbTe-Ag_2Te BNSLs due to the synergistic effects of nanoparticles (Fig. 3).[72] This observation demonstrates that nanocrystals can behave as dopants in nanoparticle-based materials. Shevchenko and co-workers reported the fluorescence spectroscopy study of long-range ordered BNSLs of CdSe and Au nanoparticles.[78] A considerably decreased fluorescence and a shortened fluorescence lifetime of the CdSe nanoparticles were observed due to the energy transfer to surrounding Au nanoparticles. Despite these contributions, the exploration of new collective properties and application in devices are unmatched to the diversity of BNSLs.

3. Honeycomb-patterned macroporous structures

3.1. Breath figure templating method

Ordered macroporous structures have received great interest in recent years because of their potential applications in many areas,

such as photonic crystals,[95] cell cultures,[96] and dye-sensitized solar cells.[97] The fabrication of these macroporous structures usually involves templating. Various templating methods have emerged based on self-assembly.[98] Since the first report by Widawski *et al.* in 1994,[99] the breath figure method has been developed as an effective templating technique for fabricating honeycomb-patterned macroporous structures.

The fabrication process of the breath figure method is described as follows: after casting a solution in a volatile solvent that is immiscible with water under high relative humidity, the rapid evaporation of the solvent decreases the air/solution interfacial temperature below its dew point, resulting in the condensation of monodisperse micrometre-sized water droplets on the surface of the solution. While the condensed water droplets do not coalesce together but are effectively stabilized by the solutes, they self-assemble into well-ordered hexagonal arrays under the effects of capillary convections. With the evaporation of solvent, the solutes precipitate around the organized water droplets. When the solvent and water droplets evaporate completely, the imprint of the water droplets is left in the dried film and 2D or 3D honeycomb-patterned macroporous structures are obtained. The water droplets act as a dynamic template here and thus the breath figure method is also called the water droplet templating method.

Several key factors appear to influence the formation of ordered macroporous structures based on the breath figure method: (i) Relative humidity. High relative humidity in the fabrication conditions is essential and can be achieved by passing a moist airflow across the sample solution or using specially-controlled high relative humidity chambers. It should be noted that ordered honeycomb structures are formed at the air/water interface without the use of moist airflow or humidity chambers.[100] Relative humidity is sometimes one criterion for discerning the breath figure mechanism of pore structure formation from other mechanisms. (ii) Solvent. Although many volatile solvents have been used to prepare macroporous structures, the most used solvents for formation of high quality honeycomb structures are carbon disulfide (CS_2) and chloroform ($CHCl_3$). Besides the low boiling point (46 °C for CS_2 and 61 °C for $CHCl_3$), one important common feature of the two solvents should be the low water miscibility (0.005% for CS_2 and 0.056% for $CHCl_3$, expressed by the solubility of water in the solvent). Which solvent will work well for a specific system may depend on the materials used to fabricate the porous structures. It should also be noted that ordered honeycomb structures are reported to be formed when tetrahydrofuran (THF, miscible with water) is used as the solvent and several groups have declared that this is also based on the breath figure mechanism.[101–104] (iii) Stabilization of water droplets. While the immiscibility of solvent with water enables the presence of a water phase in the solution, stabilization of water droplets preventing coalescence is crucial for the formation of closed-packed templating arrays of water droplets. However, there remains a lack of quantitative understanding of the stabilization mechanism in the formation process of breath figures.

In fact, the final structure morphology or quality depends on many influencing parameters, such as concentration, humidity, type of materials, and molecular weight.[105] Generally, higher concentration gives rise to smaller pore sizes. Furthermore, higher relative humidity gives larger pore sizes while increased polymer molecular weight has given larger pore sizes as well.[106]

3.2. New building blocks

Due to the simplicity of fabrication (eliminating the need for multiple assembly steps which are involved in the conventional templating methods), the breath figure method has stimulated wide interest. A variety of materials have been exploited as building blocks, such as homopolymers, copolymers, star polymers, amphiphilic polyion complex, and metal nanoparticles, which have been summarized in a review by Bunz in 2006.[107] Recently, new building blocks for fabricating ordered honeycomb structures using the breath figure method have emerged.[108]

3.2.1. Polymer hybrids. As mentioned above, formation of breath figure arrays requires that the solutes prevent water droplet coalescence. Numerous studies have shown that this requirement can be met by use of polymers with an amphiphilic nature.[109,110] Both amphiphilic copolymers[111–114] and homopolymers with polar groups at the chain ends[115–119] tend to stabilize the condensing water droplets against coalescence (Fig. 4). Shimomura and co-workers have well shown that amphiphilic copolymers can be used as a second component or additives to induce the formation of honeycomb structures with hydrophobic polymers.[120–124] Hierarchically micro- and nanostructured polymer surfaces were obtained using block copolymer/homopolymer blends.[125] Fukuhira and co-workers reported that phospholipids were used as biocompatible surfactants for the formation of biodegradable honeycomb-patterned films and proposed that interfacial tension between a water droplet and the polymer solution governs the

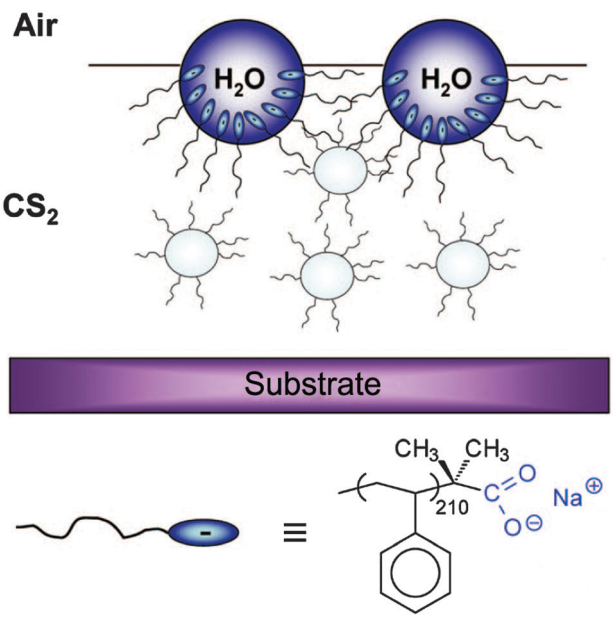

Fig. 4 Amphiphilic copolymer-stabilized water droplets condensed on the solution surface. Reproduced with permission from ref. 119, copyright 2009 American Chemical Society.

formation of honeycomb patterns.[126,127] Nomura and co-workers reported the fabrication of honeycomb-patterned thin films of PS and amphiphilic calixarene derivatives.[128]

3.2.2. Sterically-stabilized nanoparticles. Wu *et al*. and our group have shown that surfactant-encapsulated polyoxometalate (POM) clusters are a new type of building block for fabrication of honeycomb structures.[129–135] A series of hydrophobic surfactant-encapsulated clusters prepared from polyoxometalates with different compositions, shapes, and sizes, are able to self-assemble into ordered honeycomb structures.[130,134] Sakatani and co-workers reported the fabrication of macroporous films using surfactant-modified nanoparticles (SiO_2, TiO_2, Co, and CdS) based on the breath figure method.[136] Hierarchically porous materials made of metallic oxides, metals, or chalcogenides can be obtained through calcinations of the macroporous films. Xu *et al*. also reported that hierarchically ordered 2D architectures can be prepared from various nanocrystal building blocks.[137] Nakashima and co-workers reported that honeycomb structures were spontaneously formed using lipid complexes of single-walled carbon nanotubes (CNTs).[138,139] After removing the cationic ammonium lipid through ion exchange, conducting thin films with honeycomb structures were obtained.

3.2.3. Polymer nanocomposites. Polymer matrixes provide scaffolds to position and organize nanoparticles into arrays or patterns while doping of nanoparticles can conversely functionalize polymer materials. Thus polymer nanocomposites are good building blocks for fabrication of nanostructured materials. Böker and co-workers pioneered the formation of honeycomb structures of polymer nanocomposites.[140] CdSe nanoparticles doped in a casting solution of polystyrene (PS) concentrated at the interior surface of spherical cavities and decorated the honeycomb films through a hierarchical self-assembly process. The loading of nanoparticles does not apparently change the size scales and characteristics of the hexagonal arrays (Fig. 5). Nurmawati and co-workers reported that honeycomb structures of an amphiphilic conjugated polymer could be used as scaffolds to direct the self-assembly of nanomaterials (metallic nanoparticles, CNTs and C_{60}) into 2D arrays.[141] The nanoparticles were homogeneously distributed within the walls of honeycomb structures. The sizes of the breath figure cavities were reduced as the nanoparticle loading increased. Yu and co-workers reported the fabrication of macroporous films of conducting polymers (polyaniline) and Fe_3O_4 nanoparticles.[142] Lee and co-workers reported the preparation of macroporous polymer/CNT nanocomposite films using multi-walled CNTs dispersed by amine-terminated PS as building blocks.[143]

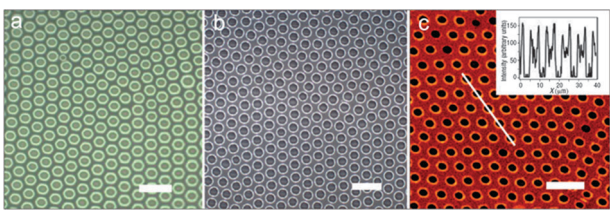

Fig. 5 Optical and confocal fluorescence microscope images of breath figures. (a) Breath figure pattern obtained with pure PS. (b) Optical and (c) confocal fluorescence microscope images of PS/CdSe nanocomposite films. Scale bars: 16 μm. The inset in c shows a fluorescence intensity scan along the line indicated. Reproduced with permission from ref. 140, copyright 2004 Nature Publishing Group.

The interfacial activities of nanoparticles can be used to direct the formation of breath figures by stabilizing the water droplets condensed on the surface of the casting solution. Ji and co-workers reported that hierarchical honeycomb structures of polymer and silica nanoparticles were formed through the combination of Pickering emulsions and capillary flow in the formation process of breath figures.[144] Similarly, surfactant-encapsulated POM clusters[145] and surface-modified zeolite crystals[146] have been used to direct the formation of polymer nanocomposite honeycomb structures. Recently, we reported that hydrophobic gold nanoparticles can stabilize the breath figures and highly ordered macroporous honeycomb films of PS and gold nanoparticles are obtained.[147] Other sterically-stabilized nanoparticles (Fe_3O_4 or QDs) can be doped into the hybrid matrix to functionalize the films.

Preparation of polymer nanocomposites either utilized the *ex situ* approach, where the pre-synthesized nanoparticles were loaded in the polymer matrixes, or the *in situ* approach, where the nanoparticle precursors were loaded and nanoparticles were synthesized by subsequent treatments. Wang and co-workers reported that honeycomb-patterned polymer/QDs composite films were fabricated from PMMA/$Cd(AA)_2$ ionomers using the breath figure method.[148] Jiang and co-workers also reported the *in situ* preparation of Ag nanoparticles and the fabrication of polymer nanocomposite films with ordered porous surface pattern.[149]

3.2.4. Small molecules. Formation of macroporous honeycomb structures using polymers, nanocomposites, and hybrids have been well studied. However, there are few studies about the fabrication of honeycomb structures using small molecules as building blocks by the breath figure method. Kim and co-workers firstly reported the application of breath figure method to a small molecule (Scheme 1).[150] This photo-responsive organogelator self-assembled into supramolecular fibrillar networks and further a hierarchically ordered honeycomb structure. Babu and co-workers also reported the formation of hierarchical macroporous structures from an amino acid linked π-conjugated organogelator.[151] Recently, a new organogelator was synthesized and large-scale ordered honeycomb patterns were also observed.[152]

3.3. Patterning on unusual substrates

3.3.1. Non-planar substrates. Fabrication of honeycomb structures by the breath figure method was usually performed on flat substrates, such as glass slides, silicon and mica wafers.

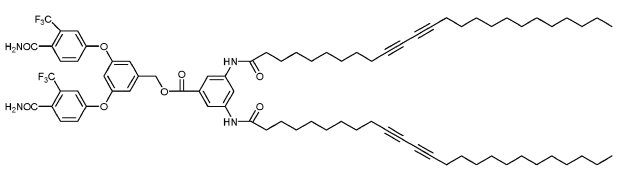

Scheme 1 Molecular structure of the organogelator that forms honeycomb structures.[150]

It has been reported that the type of substrate can affect the pattern morphology.[113,118] Connal and Qiao reported the preparation of porous polymer films with honeycomb structures on non-planar substrates using a core-cross-linked star polymer, which has an extremely low glass-transition temperature (T_g).[153,154] TEM grids were used as the non-planar substrates and the flexible honeycomb films prepared from poly(dimethyl siloxane) (PDMS) could contour the surface of the TEM grids. Furthermore, these patterned materials were used as soft lithography templates to produce corresponding negative patterns. They have also reported the successful formation of honeycomb films on particulate surfaces (Fig. 6).[155] The soft nature of the PDMS chains enables the polymer film to conform to the shape of the substrate and retain the honeycomb structures. Subsequent investigation of a range of star polymers with different compositions showed that only star polymers with a T_g below 48 °C could form homogeneous honeycomb films on non-planar substrates.[156] Recently, Li and co-workers also reported the formation of micro-patterned films with a triblock polymer (polystyrene-*b*-polyisoprene-*b*-polystyrene) on non-planar substrates.[157] Goedel and co-workers reported the preparation of micro-sieves with a hierarchical pore structure using a layer of spherical glass beads as structured substrates.[158]

3.3.2. Air/water interface. Shimomura and co-workers reported the fabrication of honeycomb-patterned macroporous films at the air/water interface by depositing a solution of an amphiphilic polymer on a water surface.[159] Formation of a polymer monolayer at the air/water interface prevents the full spreading of solution and enables the formation of breath figures on it. Fabrication of honeycomb films at the air/water interface seems to be confined to the use of amphiphilic copolymers.[141,160] We have shown that ordered honeycomb structures can also be prepared at the air/water interface using surfactant-encapsulated POM clusters as building blocks.[132–135] Breath figure templated microstructures were formed at the ambient conditions without using a closed chamber, or any adjusting of humidity. Recently, we proposed a two-step procedure for the fabrication of honeycomb structures from hydrophobic materials by forming a surfactant monolayer at the air/water interface, and depositing the casting solution onto the surfactant monolayer.[100] Freestanding polymer nanocomposite honeycomb films were also prepared using the proposed strategy (Fig. 7).[161] Through-pore structures are easily obtained in the films formed at the air/water interface.

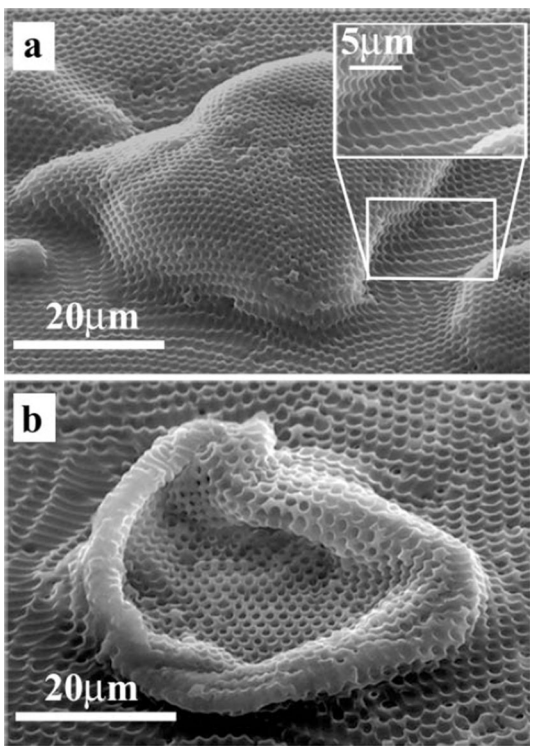

Fig. 6 SEM images of a sugar crystal coated with star PDMS honeycomb film (a), and the structure after dissolution of the sugar crystal (b).[155]

3.4. Post-fabrications and applications

3.4.1. Tailored surface functions *via* grafting. Towards the applications of honeycomb films, building blocks with certain functions are preferred to be used.[162,163] For example, honeycomb films prepared from amphiphilic polymers containing cell adhesive ligands have shown bioactivity and can be used as cell culture substrates.[164] Besides the inherent properties of building blocks, surface modification after the film formation will impart new functions. One way to surface modification is grafting to the functional groups on the film surface. Several studies have shown that the functional groups existing either on the hydrophilic block[111,165] or chain-end[117,166] of the polymers are enriched in the inner surface of pores, which makes site-directed surface modification possible.

Stenzel and co-workers reported the surface grafting onto honeycomb films which were prepared using an amphiphilic block copolymer (PS_{320}-*b*-PAA_{500}).[167] The arrangement of polymer is believed to result in the formation of hydrophilic pores and hydrophobic surface. The functional groups (–COOH) inside the hydrophilic pores are modified by covalent attachment of biotin. The surface modified honeycomb films were then used to obtain protein arrays by selective immobilization of streptavidin in the pores based on the well-established biotin–avidin system. They also reported the grafting

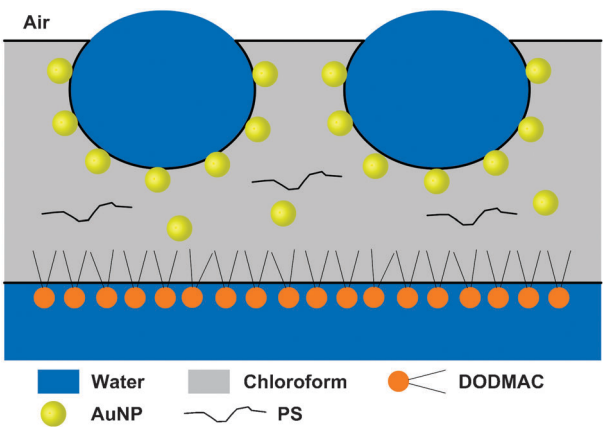

Fig. 7 Schematic illustration of the interfacial self-assembly of honeycomb structures at an air/water interface.[161]

of thermo-responsive polymer chains onto honeycomb films *via* RAFT polymerization.[168,169] The grafted films were employed for cell attachment[168] and lectin recognition.[169] Biomolecules can also be grafted onto honeycomb films which were prepared from either block copolymer[170] or star polymer[171] by ATRP. To avoid protein absorption on the top surface of the film, Zhang and Wang protected the surface with poly(ethylene glycol) by contact printing a PEG-coated PDMS film onto the porous film.[172] Subsequent attachment of glutaraldehyde to the functional groups ($-NH_2$) of an amphiphilic linear polymer directed the 3D patterning of proteins inside the pores.

3.4.2. Stability improvement *via* cross-linking. Chemical and thermal stabilities of the honeycomb-structured films are required for their application in many fields.[173] Chemical cross-linking of polymers or small molecules inside the films could lead to improved physical properties and stability of honeycomb films.[174] Bunz and co-workers reported a cross-linked polymer honeycomb film prepared by thermal-induced cross-linking of azide-substituted poly(*p*-phenyleneethynylene).[175] The interconnected air bubble arrays became isolated holes due to the collapse of the polymer matrix upon heating. The cross-linked film shows high thermal stability. Shimomura and co-workers reported that honeycomb-patterned films with controlled pore sizes could be prepared by photo (UV irradiation) cross-linking of a bisphenol A oligomer derivative.[176] After complete cross-linking by annealing, the films were insoluble to many solvents. Long *et al.* also reported solvent resistant honeycomb films from a star polymer by photo cross-linking.[177]

The 3D spherical pore structures in the films prepared by Bunz *et al.* and Shimomura *et al.* collapsed during cross-linking. Karthaus and co-workers reported two cross-linked honeycomb films in which the 3D porous structures were well retained. One is prepared by photo cross-linking of poly(vinyl cinnamate) and is stable against common organic solvents.[178] Another is prepared by chemical cross-linking of maleic anhydride groups with an alkyldiamine (Scheme 2) and shows increased thermal and solvent stability.[179] While cross-linkable groups are indispensable for photo cross-linking, Li and co-workers reported cross-linking of PS contained honeycomb films by deep UV irradiation.[180–182] Recently, Wong and co-workers reported the preparation of honeycomb films with improved mechanical properties from two silicone-based branched co-polymers.[183] Cross-linking of alkoxysilane functional groups by the sol–gel process gives stable and flexible films with good thermal conductivity.

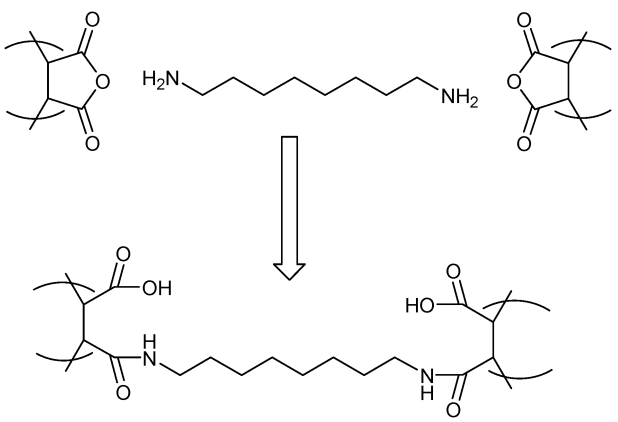

Scheme 2 Chemical cross-linking of maleic anhydride groups with an alkyldiamine.[179]

Cross-linking induced improvement of stability allows the creation of hierarchical honeycomb structures through the combination of the breath figure method and the photo-lithographic technique. Qiao and co-workers prepared multifaceted porous polymer films from cross-linkable star polymers by photo-lithographical patterning of honeycomb films.[154] Kim and co-workers reported dual-patterned honeycomb lines of a photo-responsive small molecule, which were expected to find interesting applications in photonics.[150] Recently, Shimomura and co-workers[184,185] reported the photo-patterning of honeycomb films prepared from an amphiphilic copolymer based on the molecular polarity change of spiropyran after UV irradiation.

3.4.3. Converting hybrid films into inorganic materials. Organic/inorganic hybrid honeycomb films can be prepared from organometallic polymers, polymer nanocomposites, polymer blends with inorganic precursors, and low-molar-mass metal complexes. Calcination or pyrolysis can convert the hybrid films into inorganic materials while in most cases cross-linking permits to preserve the honeycomb structures.[186] Bunz *et al.* prepared solvent resistant ceramic honeycomb structures by pyrolysis of organometallic polymer films at 500 °C under either nitrogen or air.[187] Ceramic honeycomb structures were also reported by Chen and co-workers using a ceramic precursor contained copolymer.[188] Due to low silica content, the wall was greatly thinned and only a skeleton remained after calcination at 600 °C under air. Kim and co-workers prepared highly entangled cellular CNT scaffolds which showed high electrical conductivity and field-emission properties.[143] Zhao and co-workers reported a vapor phase hydrothermal process to modify a honeycomb structured PS/TTIP (titanium tetraisopropoxide) hybrid film. Photo-active TiO_2 films were obtained after removing the organic components by pyrolysis.[189] Karthaus and co-workers[190] reported the preparation of honeycomb structured zinc oxide films, which showed increased photocatalytic activity as compared to unstructured films. Li and co-workers[191,192] reported the applications of catalytically active inorganic honeycomb structures converted from polymer/functional precursor hybrid films in fabrication of CNT and ZnO nanorod arrays (Fig. 8).

3.4.4. Physical processing. Honeycomb-structured macroporous films were used as templates for several patterned structures.[193–196] For 2D interconnected air bubble arrays, a double-layered structure supported by pillars at the vertexes of the honeycomb hexagons, pincushion structures could be fabricated by peeling off the top layer of the honeycomb structured films with adhesive tape (Fig. 9).[121,123] Shimomura and co-workers have shown well that pincushion-structured films could be used as templates for micro lens arrays,[120] superhydrophobic surfaces,[124,197,198] and SERS substrates.[199]

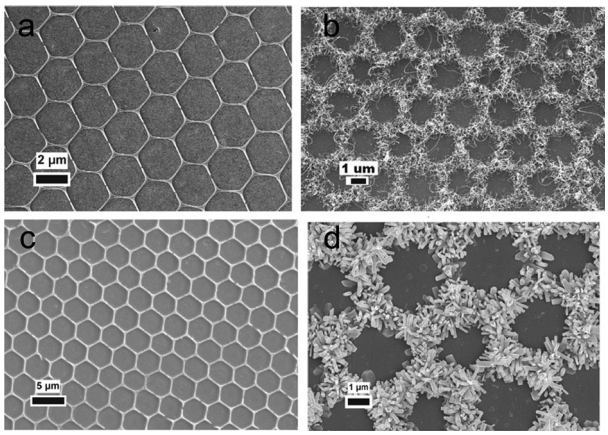

Fig. 8 SEM images of honeycomb structures of (a) ferrous, (b) CNT arrays, (c) ZnO, and (d) ZnO nanorod arrays. Reproduced with permission from ref. 191, copyright 2009 American Chemical Society.

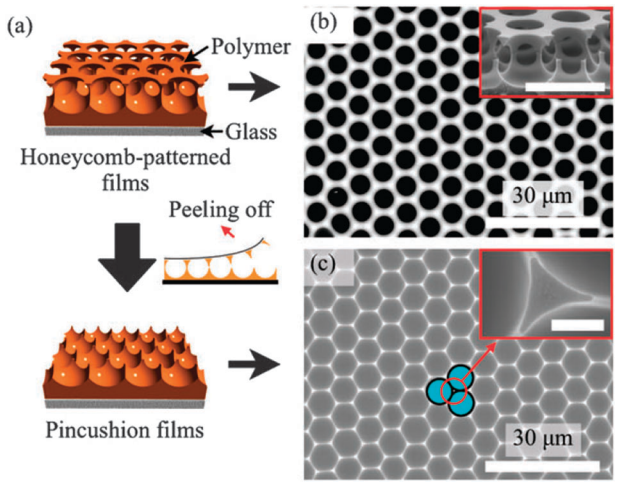

Fig. 9 (a) Schematic illustration of the preparation of pincushion structures by peeling off the top layer with adhesive tape. (b) The SEM image of the honeycomb-patterned film and (c) the SEM image of the prepared pincushion structures.[199]

Stretching and shrinking are simple processing methods for mechanical transformation of the pore shape and size of honeycomb-patterned films. Nishikawa and co-workers reported that various geometric patterns (elongated hexagons, rectangles, squares, and triangles) could be formed by mechanical stretching of honeycomb films made of a viscoelastic polymer on a water surface.[200] Yabu and co-workers showed that highly oriented deformed structures, such as nano-pit arrays, could be prepared by shrinking of honeycomb-patterned films on a thermally shrinkable substrate.[201]

4. Coffee rings

4.1. Coffee-stain-like patterns

The drying of a sessile drop containing nonvolatile solutes on a surface is a simple and appealing way to fabricate intriguing surface patterns and structures. When a spilled drop of coffee dries on a solid surface, a dense, ring-like stain is formed along the perimeter of the drop, which is commonly known as the "coffee stain effect". Coffee-stain-like ring patterns are always observed in evaporative deposition from colloidal suspensions. Deegan and co-workers ascribe the coffee-ring like pattern formation to a form of outward capillary flow.[202] The model is based on the conditions that (i) the solvent wets the surface well and (ii) the gas–liquid–solid contact line is pinned. Since the solvent evaporation rate is the greatest at the edge, pinning of the contact line of the drying drop results in an outward flow to replenish the evaporative losses. The outward flow carries the dispersed particles from the interior to the edge of the drop and deposits them at the perimeter of the drop forming a solid ring.[203] They also found that mechanisms typically responsible for solute transport, such as surface-tension gradients, solute diffusion, electrostatic and gravity effects, are negligible in the process of ring formation. Consequently this geometrical constraint related phenomenon is not restricted to typical colloidal particles but can be applied to a wide variety of materials, including nanoparticles,[204] polymers,[205,206] bacteria,[207,208] and DNA.[209]

In Deegan's model, pinning of the contact line is the premise of ring pattern formation. Contact line pinning is generally associated with surface heterogeneities of the substrate. However, the coffee stain effect is also observed from drying drops of aqueous suspensions on smooth surfaces, such as freshly cleaved mica.[210] Apparently the substrate by itself cannot keep the contact line pinned indefinitely. Deegan demonstrated that the drop itself can generate the pinning of the contact line and referred to this process as "self-pinning": the contact line was anchored temporarily by some preexisting conditions and then was pinned by accumulation of solid components, which increases the energy barrier the contact line must surmount before retreating.[210] While contact line pinning is well accepted as the cause of ring pattern formation on hydrophilic substrates, Sommer and Rozlosnik obtained rings on strongly hydrophobic substrates and proposed that contact line pinning is not causal for ring formation, but rather that the convective flow carrying the particles to the perimeter contributes to the anchoring of nanoparticles at the edge of the drop.[211] In fact, in the case of hydrophobic surfaces possessing a larger contact angle for water, the pattern formation becomes more complex.[212]

Numerous studies have been devoted to investigating the mechanism and influencing parameters of ring stain formation. Maenosono and co-workers reported the formation of ring-shaped arrays of semiconductor nanoparticles and found that the ring width depends on the particle volume fraction.[204] Chon and co-workers studied the effect of nanoparticle size on formation of ring-shaped nanoparticle patterns from strongly pinned nano-fluid droplets.[213] Smaller nanoparticles result in relatively wider edge accumulation, whereas larger nanoparticles give rise to narrower and more distinctive ring stains. Sangani and co-workers determined the capillary force on the particles near a drop edge and found that not all particles are effective in pinning the contact line.[214] They proposed a criterion that must be satisfied for particles to form the ring-like patterns. According to the criterion, whether the particles facilitate the pinning of the contact line depends not only on the particle size but also on particle concentration, drop radius, evaporation rate, and the wetting characteristics of the substrate.

While the typical solute transport mechanisms can be negligible in Deegan's model for the case of a single phase of particles in water droplets, these mechanisms become dominating in the case of organic fluids or multi-phase solutions.[215] Hu and Larson experimentally and theoretically demonstrated that evaporation induced thermal Marangoni flows can reverse the coffee stain effect, as a result of which depositing the particles at the center rather than the edge of the droplet.[216] Park and Moon also showed the competition between the convective and Marangoni flows based on that particle deposit patterns can be controlled by using a mixture of low-boiling-point and high-boiling-point solvents.[217] The Marangoni effect can also be caused by the gradient of the solute concentration. Kajiya and co-workers reported that in drying the droplets containing polymer whose surface tension has a negative dependence on the polymer concentration, the concentration Marangoni effect can induce the recession of the contact line and a volcano-like profile is formed.[218] They also reported that the drying process of the polymer solution is strongly affected by the addition of surfactants.[219] The Marangoni flow induced by inhomogeneous distribution of the surfactant changes the profile of the dried polymer film from a ring-like profile to a flat profile. Nguyen and Stebe also reported that surfactants can be used to alter the internal flows and deposition patterns from evaporating aqueous drops of small particles.[220,221] In this sense, formation of coffee-ring patterns requires not only the pinning of the contact line but also suppression of the Marangoni effect.

Coffee-stain-like ring patterns can form both on the macroscale[222] (on the order of millimetres) and microscale,[223] in which the latter case has potential applications in biomolecular sensing and medical diagnosis. Before we can take advantage of the coffee stain phenomenon on smaller length scales, it is necessary to understand the natural size limit of rings. Recently Shen and co-workers investigated the drying behavior of water-based droplets with sizes ranging from millimetres down to a few micrometres to determine the size of the smallest droplet that results in a coffee ring.[224] They found that there exists a droplet size limit for the formation of a coffee ring structure when the particle concentration is above a threshold value. For latex particles of $\sim$100 nm in size, the minimum diameter of the coffee ring structure is found to be $\sim$10 μm (Fig. 10). As the droplet size decreases, the time scale of the liquid evaporation becomes competitive to that of particle movement. When the droplet evaporates much faster than the particle movement, coffee ring formation is inhibited.

Although the coffee stain effect in the drying of a sessile drop is undesirable in some cases that need a uniform distribution of solutes,[225,226] this commonly observed phenomenon in our daily life has been used as a technique for the assembly of nanoparticles and other materials.[227,228] Magdassi and co-workers reported the self-assembly of silver nanoparticle rings with high electrical conductivity based on the coffee stain effect.[229] They also demonstrated the fabrication of transparent conductive patterns (2D array of interconnected metallic rings) through the combination of the coffee stain effect and inkjet printing.[230] On the basis of the coffee stain effect, Choi and co-workers developed a patterning technique to produce 3D assemblies of micro and nanoparticles.[231]

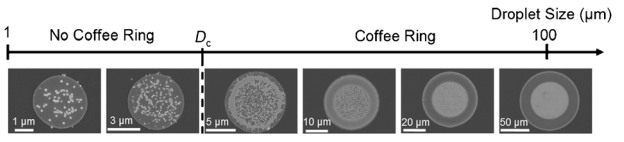

Fig. 10 SEM images of nanoparticle deposit patterns with increasing droplet sizes (left to right). Reproduced with permission from ref. 224, copyright 2010 American Chemical Society.

4.2. Concentric multiple rings

One of the critical conditions for the formation of coffee-rings along the perimeter of drying droplets is the pinning of the contact line. However, in some cases the contact line is not kept pinned during the whole drying process but can move at a certain stage of drying. It has been reported that the contact line shows a stick–slip motion (repeated pinning and depinning).[210,232–236] When this happens, concentric multiple rings are formed.

Adachi and co-workers observed the formation of multiple rings caused by stick–slip motion of the contact line and proposed that the stick–slip motion is caused by the competition between friction and surface tension.[232] Deegan further investigated the pattern formation and found that small particles (0.1 μm in diameter) were sometimes observed to form concentric rings but larger particles (1 μm in diameter) were not.[210] Shmuylovich and co-workers reported sequent pinning–depinning of the contact line and the formation of concentric rings of both small (0.88 μm in diameter) and large (3.15 μm in diameter) latex particles.[233] Zhu and co-workers observed the formation of multiple ring patterns of DNA (Fig. 11) and attributed it to the generation of new contact lines which is caused by stagnation flow inside the current contact line.[234] They also examined the pattern formation of multi-component systems using a DNA-colloid binary suspension as a model system. High DNA concentration and low colloidal concentration favor the formation of the multiple ring patterns. Increase of particle size can disrupt smooth multiple rings to form complex irregular patterns.[235]

Generally the concentric ring patterns from drying mediated self-assembly are irregular due to the essentially stochastic pinning–depinning cycles of the contact line motion. Lin and co-workers developed a robust self-assembly method for

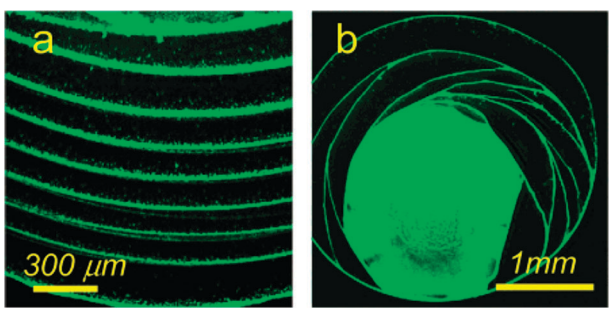

Fig. 11 Fluorescent micrographs of typical DNA multiple-ring pattern formed by evaporation of DNA droplets with different initial DNA concentrations. Reproduced with permission from ref. 235, copyright 2008 American Chemical Society.

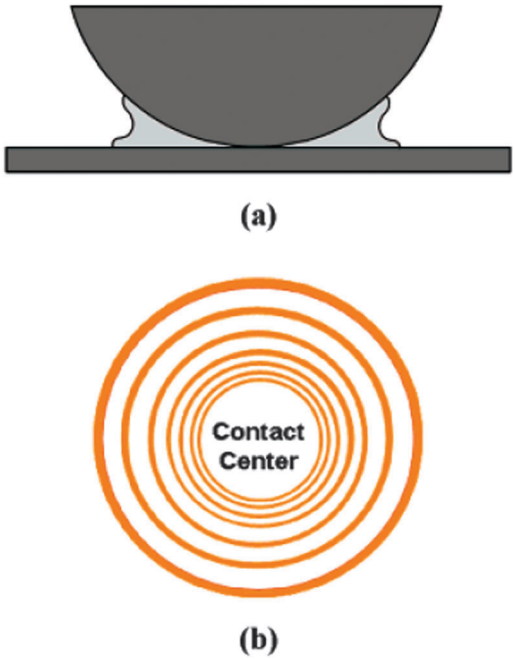

Fig. 12 Schematic illustration of an evaporating droplet confined in a sphere-on-flat geometry (a) and the formed gradient concentric ring patterns (b). Reproduced with permission from ref. 246, copyright 2006 American Chemical Society.

highly ordered gradient concentric ring patterns by controlling the drop evaporation in confined geometries, such as sphere-on-flat geometry (Fig. 12).[237,238] The confined geometry leads to the formation of a capillary bridge of the solution and enables the motion of the contact line in a controlled, consecutively stick–slip manner.[239] Both polymers and nanoparticles have been used as building blocks to produce concentric rings using this simple, one-step technique.[240–242] By changing the shape of the upper surface of a confined geometry, highly ordered periodic complex structures, such as squares,[243] triangular contour lines,[243] and straight or jagged stripes,[244] are obtained. Moreover, the periodic ring structures have been used as templates to direct the formation of gradient concentric rings of metal, metal oxide, and carbon nanotubes.[245–247]

5. Concluding remarks

Ordered patterns and structures at the nanoscale (superlattices), mesoscale (honeycomb structures) and macroscale (coffee rings) are formed *via* "bottom-up" interfacial self-assembly. Compared with molecular self-assembly, which is based on non-covalent interactions, nanocrystal-involved interfacial self-assembly gives rise to patterns on relatively large scales. In these scales, the weak interactions that are driving forces for molecular self-assembly become less important and various long-range forces, such as interfacial interactions and capillary forces, become dominating (Fig. 13). Formation of nanocrystal superlattices is mainly driven by various interparticle interactions and entropy potential. The variety of driving forces gives rise to rich superlattice structures. Capillary forces and convection effects combining with interfacial interactions

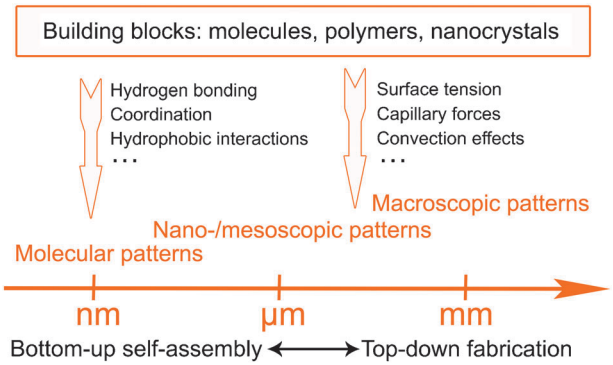

Fig. 13 Comparison of the driving forces between the self-assembled patterns on different length scales.

bring about even larger scale surface patterns, honeycomb structures and coffee rings.

While self-assembly is the only practical approach for creating a variety of nanostructures, it also shows great superiority in building hierarchical structures through the combination of interactions on different length scales. However, the interplay of the different forces at larger scales is truly complex. To achieve highly ordered reproducible patterns or structures in large areas, it requires a rigorous control over many fabricating parameters. In contrast, "top-down" fabrications have a high level of control over the precision of patterns on large scales. Thus combination of interfacial self-assembly with some "top-down" techniques, such as photolithography, will create more complex structures and undoubtedly will find widespread use in the near future.

Acknowledgements

Financial support from the National Basic Research Program of China ("973" Program, 2009CB930103) and the NSFC (21033005).

Notes and references

1 J. M. Lehn, *Proc. Natl. Acad. Sci. U. S. A.*, 2002, **99**, 4763–4768.
2 S. Zhang, *Nat. Biotechnol.*, 2003, **21**, 1171–1178.
3 A. K. Boal, F. Ilhan, J. E. DeRouchey, T. Thurn-Albrecht, T. P. Russell and V. M. Rotello, *Nature*, 2000, **404**, 746–748.
4 S. Leininger, B. Olenyuk and P. J. Stang, *Chem. Rev.*, 2000, **100**, 853–908.
5 J. D. Hartgerink, E. Beniash and S. I. Stupp, *Science*, 2001, **294**, 1684–1688.
6 E. Winfree, F. Liu, L. A. Wenzler and N. C. Seeman, *Nature*, 1998, **394**, 539–544.
7 J. H. Fendler, *Chem. Mater.*, 2001, **13**, 3196–3210.
8 B. Amir Parviz, D. Ryan and G. M. Whitesides, *IEEE Trans. Adv. Packag.*, 2003, **26**, 233–241.
9 C. T. Black, R. Ruiz, G. Breyta, J. Y. Cheng, M. E. Colburn, K. W. Guarini, H. C. Kim and Y. Zhang, *IBM J. Res. Dev.*, 2007, **51**, 605–633.
10 H. Otsuka, Y. Nagasaki and K. Kataoka, *Curr. Opin. Colloid Interface Sci.*, 2001, **6**, 3–10.
11 S. Zhang, D. M. Marini, W. Hwang and S. Santoso, *Curr. Opin. Chem. Biol.*, 2002, **6**, 865–871.
12 M. Weis, C. Waloch, W. Seiche and B. Breit, *J. Am. Chem. Soc.*, 2006, **128**, 4188–4189.
13 T. Arai, Y. Yamada, N. Yamamoto, H. Sasai and M. Shibasaki, *Chem.–Eur. J.*, 1996, **2**, 1368–1372.

14 M. N. Stojanovic, P. de Prada and D. W. Landry, *J. Am. Chem. Soc.*, 2000, **122**, 11547–11548.
15 X. Yang, S. Johnson, J. Shi, T. Holesinger and B. Swanson, *Sens. Actuators, B*, 1997, **45**, 87–92.
16 H. Yang, C. Yu, Q. Song, Y. Xia, F. Li, Z. Chen, X. Li, T. Yi and C. Huang, *Chem. Mater.*, 2006, **18**, 5173–5177.
17 S. P. Jiang, Z. Liu and Z. Q. Tian, *Adv. Mater.*, 2006, **18**, 1068–1072.
18 S. C. Glotzer and M. J. Solomon, *Nat. Mater.*, 2007, **6**, 557–562.
19 Z. Nie, W. Li, M. Seo, S. Xu and E. Kumacheva, *J. Am. Chem. Soc.*, 2006, **128**, 9408–9412.
20 S. Sacanna, W. T. M. Irvine, P. M. Chaikin and D. J. Pine, *Nature*, 2010, **464**, 575–578.
21 M. J. Solomon, *Nature*, 2010, **464**, 496–498.
22 D. Li, M. B. Müller, S. Gilje, R. B. Kaner and G. G. Wallace, *Nat. Nanotechnol.*, 2008, **3**, 101–105.
23 J. Bigot, B. Charleux, G. Cooke, F. Delattre, D. Fournier, J. Lyskawa, L. Sambe, F. Stoffelbach and P. Woisel, *J. Am. Chem. Soc.*, 2010, **132**, 10796–10801.
24 B. Trappmann, K. Ludwig, M. R. Radowski, A. Shukla, A. Mohr, H. Rehage, C. Böttcher and R. Haag, *J. Am. Chem. Soc.*, 2010, **132**, 11119–11124.
25 D. Chakrabarti, S. N. Fejer and D. J. Wales, *Proc. Natl. Acad. Sci. U. S. A.*, 2009, **106**, 20164–20167.
26 R. F. Service, *Science*, 2005, **309**, 95.
27 K. Ariga, J. P. Hill, M. V. Lee, A. Vinu, R. Charvet and S. Acharya, *Sci. Technol. Adv. Mater.*, 2008, **9**, 014109.
28 G. M. Whitesides, J. P. Mathias and C. T. Seto, *Science*, 1991, **254**, 1312–1319.
29 G. Whitesides and M. Boncheva, *Proc. Natl. Acad. Sci. U. S. A.*, 2002, **99**, 4769–4774.
30 M. Boncheva and G. M. Whitesides, *MRS Bull.*, 2005, **30**, 736–742.
31 C. M. Drain, A. Varotto and I. Radivojevic, *Chem. Rev.*, 2009, **109**, 1630–1658.
32 G. M. Whitesides and B. Grzybowski, *Science*, 2002, **295**, 2418–2421.
33 J. D. Halley and D. A. Winkler, *Complexity*, 2008, **14**, 10–17.
34 F. M. Menger, *Proc. Natl. Acad. Sci. U. S. A.*, 2002, **99**, 4818–4822.
35 C. F. J. Faul and M. Antonietti, *Adv. Mater.*, 2003, **15**, 673–683.
36 T. H. Rehm and C. Schmuck, *Chem. Soc. Rev.*, 2010, **39**, 3597–3611.
37 Y. Wang, H. Xu and X. Zhang, *Adv. Mater.*, 2009, **21**, 2849–2864.
38 K. Ariga, *J. Nanosci. Nanotechnol.*, 2004, **4**, 23–34.
39 K. Ariga, M. V. Lee, T. Mori, X. Y. Yu and J. P. Hill, *Adv. Colloid Interface Sci.*, 2010, **154**, 20–29.
40 A. Böker, J. He, T. Emrick and T. P. Russell, *Soft Matter*, 2007, **3**, 1231–1248.
41 S. Kinge, M. Crego-Calama and D. N. Reinhoudt, *ChemPhysChem*, 2008, **9**, 20–42.
42 C. Burda, X. Chen, R. Narayanan and M. A. El-Sayed, *Chem. Rev.*, 2005, **105**, 1025–1102.
43 M. Grzelczak, J. Pérez-Juste, P. Mulvaney and L. M. Liz-Marzán, *Chem. Soc. Rev.*, 2008, **37**, 1783–1791.
44 A. R. Tao, S. Habas and P. Yang, *Small*, 2008, **4**, 310–325.
45 D. V. Talapin, J.-S. Lee, M. V. Kovalenko and E. V. Shevchenko, *Chem. Rev.*, 2010, **110**, 389–458.
46 C. P. Collier, T. Vossmeyer and J. R. Heath, *Annu. Rev. Phys. Chem.*, 1998, **49**, 371–404.
47 Z. L. Wang, *Adv. Mater.*, 1998, **10**, 13–30.
48 B. L. V. Prasad, C. M. Sorensen and K. J. Klabunde, *Chem. Soc. Rev.*, 2008, **37**, 1871–1883.
49 S. He, J. Yao, P. Jiang, D. Shi, H. Zhang, S. Xie, S. Pang and H. Gao, *Langmuir*, 2001, **17**, 1571–1575.
50 X. M. Lin, H. M. Jaeger, C. M. Sorensen and K. J. Klabunde, *J. Phys. Chem.B*, 2001, **105**, 3353–3357.
51 E. V. Shevchenko, D. V. Talapin, C. B. Murray and S. O'Brien, *J. Am. Chem. Soc.*, 2006, **128**, 3620–3637.
52 M. I. Bodnarchuk, M. V. Kovalenko, S. Pichler, G. Fritz-Popovski, G. Hesser and W. Heiss, *ACS Nano*, 2009, **4**, 423–431.
53 M.-H. Lin, H.-Y. Chen and S. Gwo, *J. Am. Chem. Soc.*, 2010, **132**, 11259–11263.
54 W. Cheng, N. Park, M. T. Walter, M. R. Hartman and D. Luo, *Nat. Nanotechnol.*, 2008, **3**, 682–690.
55 A. Akey, C. Lu, L. Yang and I. P. Herman, *Nano Lett.*, 2010, **10**, 1517–1521.
56 Q. Zhang, J. Xie, J. Yang and J. Y. Lee, *ACS Nano*, 2009, **3**, 139–148.
57 Z. Quan and J. Fang, *Nano Today*, 2010, **5**, 390–411.
58 S. M. Rupich, E. V. Shevchenko, M. I. Bodnarchuk, B. Lee and D. V. Talapin, *J. Am. Chem. Soc.*, 2010, **132**, 289–296.
59 T. P. Bigioni, X. M. Lin, T. T. Nguyen, E. I. Corwin, T. A. Witten and H. M. Jaeger, *Nat. Mater.*, 2006, **5**, 265–270.
60 C. Lu, Z. Chen and S. O'Brien, *Chem. Mater.*, 2008, **20**, 3594–3600.
61 T. Nishio, K. Niikura, Y. Matsuo and K. Ijiro, *Chem. Commun.*, 2010, **46**, 8977–8979.
62 Y. Wang, Q. Dai, L. Wang, B. Zou, T. Cui, B. Liu, W. W. Yu, M. Z. Hu and G. Zou, *J. Phys. Chem. C*, 2010, **114**, 11425–11429.
63 C. F. Chen, H. Y. Chen, K. J. Lin and S. Gwo, *J. Am. Chem. Soc.*, 2008, **130**, 824–826.
64 A. Tao, P. Sinsermsuksakul and P. Yang, *Nat. Nanotechnol.*, 2007, **2**, 435–440.
65 A. R. Tao, D. P. Ceperley, P. Sinsermsuksakul, A. R. Neureuther and P. Yang, *Nano Lett.*, 2008, **8**, 4033–4038.
66 E. Tam, P. Podsiadlo, E. Shevchenko, D. F. Ogletree, M. P. Delplancke-Ogletree and P. D. Ashby, *Nano Lett.*, 2010, **10**, 2363–2367.
67 P. Podsiadlo, G. Krylova, B. Lee, K. Critchley, D. J. Gosztola, D. V. Talapin, P. D. Ashby and E. V. Shevchenko, *J. Am. Chem. Soc.*, 2010, **132**, 8953–8960.
68 E. V. Shevchenko, D. V. Talapin, S. O'Brien and C. B. Murray, *J. Am. Chem. Soc.*, 2005, **127**, 8741–8747.
69 D. V. Talapin, E. V. Shevchenko, C. B. Murray, A. V. Titov and P. Král, *Nano Lett.*, 2007, **7**, 1213–1219.
70 C. J. Kiely, J. Fink, J. G. Zheng, M. Brust, D. Bethell and D. J. Schiffrin, *Adv. Mater.*, 2000, **12**, 640–643.
71 C. J. Kiely, J. Fink, M. Brust, D. Bethell and D. J. Schiffrin, *Nature*, 1998, **396**, 444–446.
72 J. J. Urban, D. V. Talapin, E. V. Shevchenko, C. R. Kagan and C. B. Murray, *Nat. Mater.*, 2007, **6**, 115–121.
73 Z. Chen and S. O'Brien, *ACS Nano*, 2008, **2**, 1219–1229.
74 D. A. M. Vanmaekelbergh, J. D. Meeldijk, R. Koole, B. Nijs, W. H. Evers and K. Overgaag, *J. Am. Chem. Soc.*, 2008, **130**, 7833–7835.
75 W. H. Evers, B. D. Nijs, L. Filion, S. Castillo, M. Dijkstra and D. Vanmaekelbergh, *Nano Lett.*, 2010, **10**, 4235–4241.
76 Z. Chen, J. Moore, G. Radtke, H. Sirringhaus and S. O'Brien, *J. Am. Chem. Soc.*, 2007, **129**, 15702–15709.
77 M. V. Kovalenko, M. I. Bodnarchuk and D. V. Talapin, *J. Am. Chem. Soc.*, 2010, **132**, 15124–15126.
78 E. V. Shevchenko, M. Ringler, A. Schwemer, D. V. Talapin, T. Klar, A. L. Rogach, J. Feldmann and A. P. Alivisatos, *J. Am. Chem. Soc.*, 2008, **130**, 3274–3275.
79 E. V. Shevchenko, D. V. Talapin, N. A. Kotov, S. O'Brien and C. B. Murray, *Nature*, 2006, **439**, 55–59.
80 J. Chen, X. Ye and C. B. Murray, *ACS Nano*, 2010, **4**, 2374–2381.
81 E. V. Shevchenko, D. V. Talapin, A. L. Rogach, A. Kornowski, M. Haase and H. Weller, *J. Am. Chem. Soc.*, 2002, **124**, 11480–11485.
82 F. X. Redl, K. S. Cho, C. B. Murray and S. O'Brien, *Nature*, 2003, **423**, 968–971.
83 A. E. Saunders and B. A. Korgel, *ChemPhysChem*, 2005, **6**, 61–65.
84 D. K. Smith, B. Goodfellow, D. M. Smilgies and B. A. Korgel, *J. Am. Chem. Soc.*, 2009, **131**, 3281–3290.
85 S. Hachisu and S. Yoshimura, *Nature*, 1980, **283**, 188–189.
86 Y. S. Cho, G. R. Yi, J. M. Lim, S. H. Kim, V. N. Manoharan, D. J. Pine and S. M. Yang, *J. Am. Chem. Soc.*, 2005, **127**, 15968–15975.
87 E. C. M. Vermolen, A. Kuijk, L. C. Filion, M. Hermes, J. H. J. Thijssen, M. Dijkstra and A. van Blaaderen, *Proc. Natl. Acad. Sci. U. S. A.*, 2009, **106**, 16063–16067.
88 M. E. Leunissen, C. G. Christova, A. P. Hynninen, C. P. Royall, A. I. Campbell, A. Imhof, M. Dijkstra, R. van Roij and A. van Blaaderen, *Nature*, 2005, **437**, 235–240.
89 P. Bartlett and A. I. Campbell, *Phys. Rev. Lett.*, 2005, **95**, 128302.
90 M. D. Eldridge, P. A. Madden and D. Frenkel, *Nature*, 1993, **365**, 35–37.

91 A. M. Kalsin, M. Fialkowski, M. Paszewski, S. K. Smoukov, K. J. M. Bishop and B. A. Grzybowski, *Science*, 2006, **312**, 420–424.
92 M. I. Bodnarchuk, M. V. Kovalenko, W. Heiss and D. V. Talapin, *J. Am. Chem. Soc.*, 2010, **132**, 11967–11977.
93 C. R. Kagan, C. B. Murray, M. Nirmal and M. G. Bawendi, *Phys. Rev. Lett.*, 1996, **76**, 1517–1520.
94 H. Zeng, J. Li, J. P. Liu, Z. L. Wang and S. Sun, *Nature*, 2002, **420**, 395–398.
95 S. Kubo, Z. Z. Gu, K. Takahashi, A. Fujishima, H. Segawa and O. Sato, *J. Am. Chem. Soc.*, 2004, **126**, 8314–8319.
96 H. Sunami, E. Ito, M. Tanaka, S. Yamamoto and M. Shimomura, *Colloids Surf., A*, 2006, **284–285**, 548–551.
97 E. S. Kwak, W. Lee, N. G. Park, J. Kim and H. Lee, *Adv. Funct. Mater.*, 2009, **19**, 1093–1099.
98 M. L. K. Hoa, M. Lu and Y. Zhang, *Adv. Colloid Interface Sci.*, 2006, **121**, 9–23.
99 G. Widawski, M. Rawiso and B. Francois, *Nature*, 1994, **369**, 387–389.
100 H. Ma and J. Hao, *Chem.–Eur. J.*, 2010, **16**, 655–660.
101 M. S. Park and J. K. Kim, *Langmuir*, 2005, **21**, 11404–11408.
102 W. Madej, A. Budkowski, J. Raczkowska and J. Rysz, *Langmuir*, 2008, **24**, 3517–3524.
103 L. Cui, J. Peng, Y. Ding, X. Li and Y. Han, *Polymer*, 2005, **46**, 5334–5340.
104 A. Muñoz-Bonilla, E. Ibarboure, V. Bordegé, M. Fernández-García and J. Rodríguez-Hernández, *Langmuir*, 2010, **26**, 8552–8558.
105 J. Peng, Y. Han, Y. Yang and B. Li, *Polymer*, 2004, **45**, 447–452.
106 M. H. Stenzel, C. Barner-Kowollik and T. P. Davis, *J. Polym. Sci., Part A: Polym. Chem.*, 2006, **44**, 2363–2375.
107 U. H. F. Bunz, *Adv. Mater.*, 2006, **18**, 973–989.
108 H. Sun, W. Li and L. Wu, *Langmuir*, 2009, **25**, 10466–10472.
109 J. F. Kadla, F. H. Asfour and B. Bar-Nir, *Biomacromolecules*, 2007, **8**, 161–165.
110 T. Hayakawa, T. Kouketsu, M. Kakimoto, H. Yokoyama and S. Horiuchi, *Macromol. Res.*, 2006, **14**, 52–58.
111 A. Nygard, T. P. Davis, C. Barner-Kowollik and M. H. Stenzel, *Aust. J. Chem.*, 2005, **58**, 595–599.
112 A. E. Saunders, J. L. Dickson, P. S. Shah, M. Y. Lee, K. T. Lim, K. P. Johnston and B. A. Korgel, *Phys. Rev. E*, 2006, **73**, 031608.
113 C. Wang, Y. Mao, D. Wang, Q. Qu, G. Yang and X. Hu, *J. Mater. Chem.*, 2008, **18**, 683–690.
114 D. Beattie, K. H. Wong, C. Williams, L. A. Poole-Warren, T. P. Davis, C. Barner-Kowollik and M. H. Stenzel, *Biomacromolecules*, 2006, **7**, 1072–1082.
115 M. Srinivasarao, D. Collings, A. Philips and S. Patel, *Science*, 2001, **292**, 79–83.
116 A. Bolognesi, C. Mercogliano, S. Yunus, M. Civardi, D. Comoretto and A. Turturro, *Langmuir*, 2005, **21**, 3480–3485.
117 S. Yunus, A. Delcorte, C. Poleunis, P. Bertrand, A. Bolognesi and C. Botta, *Adv. Funct. Mater.*, 2007, **17**, 1079–1084.
118 L. Ghannam, M. Manguian, J. François and L. Billon, *Soft Matter*, 2007, **3**, 1492–1499.
119 L. Billon, M. Manguian, V. Pellerin, M. Joubert, O. Eterradossi and H. Garay, *Macromolecules*, 2009, **42**, 345–356.
120 H. Yabu and M. Shimomura, *Langmuir*, 2005, **21**, 1709–1711.
121 H. Yabu and M. Shimomura, *Langmuir*, 2006, **22**, 4992–4997.
122 M. Kojima, Y. Hirai, H. Yabu and M. Shimomura, *Polym. J.*, 2009, **41**, 667–671.
123 H. Yabu, Y. Hirai and M. Shimomura, *Langmuir*, 2006, **22**, 9760–9764.
124 H. Yabu, Y. Hirai, M. Kojima and M. Shimomura, *Chem. Mater.*, 2009, **21**, 1787–1789.
125 A. Muñoz-Bonilla, E. Ibarboure, E. Papon and J. Rodriguez-Hernandez, *Langmuir*, 2009, **25**, 6493–6499.
126 Y. Fukuhira, E. Kitazono, T. Hayashi, H. Kaneko, M. Tanaka, M. Shimomura and Y. Sumi, *Biomaterials*, 2006, **27**, 1797–1802.
127 Y. Fukuhira, H. Yabu, K. Ijiro and M. Shimomura, *Soft Matter*, 2009, **5**, 2037–2041.
128 E. Nomura, A. Hosoda, M. Takagaki, H. Mori, Y. Miyake, M. Shibakami and H. Taniguchi, *Langmuir*, 2010, **26**, 10266–10270.
129 W. Bu, H. Li, H. Sun, S. Yin and L. Wu, *J. Am. Chem. Soc.*, 2005, **127**, 8016–8017.
130 H. Sun, H. Li, W. Bu, M. Xu and L. Wu, *J. Phys. Chem. B*, 2006, **110**, 24847–24854.
131 H. Sun, W. Li, L. Wollenberg, B. Li, L. Wu, F. Li and L. Xu, *J. Phys. Chem. B*, 2009, **113**, 14674–14680.
132 D. Fan, X. Jia, P. Tang, J. Hao and T. Liu, *Angew. Chem., Int. Ed.*, 2007, **46**, 3342–3345.
133 P. Tang and J. Hao, *Langmuir*, 2010, **26**, 3843–3847.
134 P. Tang and J. Hao, *Adv. Colloid Interface Sci.*, 2010, **161**, 163–170.
135 P. Tang and J. Hao, *New J. Chem.*, 2010, **34**, 1059–1062.
136 Y. Sakatani, C. Boissière, D. Grosso, L. Nicole, G. Soler-Illia and C. Sanchez, *Chem. Mater.*, 2008, **20**, 1049–1056.
137 X. Xu, X. Wang, A. Nisar, X. Liang, J. Zhuang, S. Hu and Y. Zhuang, *Adv. Mater.*, 2008, **20**, 3702–3708.
138 H. Takamori, T. Fujigaya, Y. Yamaguchi and N. Nakashima, *Adv. Mater.*, 2007, **19**, 2535–2539.
139 N. Wakamatsu, H. Takamori, T. Fujigaya and N. Nakashima, *Adv. Funct. Mater.*, 2009, **19**, 311–316.
140 A. Böker, Y. Lin, K. Chiapperini, R. Horowitz, M. Thompson, V. Carreon, T. Xu, C. Abetz, H. Skaff, A. D. Dinsmore, T. Emrick and T. P. Russell, *Nat. Mater.*, 2004, **3**, 302–306.
141 M. H. Nurmawati, P. K. Ajikumar, R. Renu and S. Valiyaveettil, *Adv. Funct. Mater.*, 2008, **18**, 3213–3218.
142 C. Yu, J. Zhai, Z. Li, M. Wan, M. Gao and L. Jiang, *Thin Solid Films*, 2008, **516**, 5107–5110.
143 S. H. Lee, J. S. Park, B. K. Lim, C. B. Mo, W. J. Lee, J. M. Lee, S. H. Hong and S. O. Kim, *Soft Matter*, 2009, **5**, 2343–2346.
144 W. Sun, J. Ji and J. Shen, *Langmuir*, 2008, **24**, 11338–11341.
145 H. Sun, H. Li and L. Wu, *Polymer*, 2009, **50**, 2113–2122.
146 V. Vohra, A. Bolognesi, G. Calzaferri and C. Botta, *Langmuir*, 2009, **25**, 12019–12023.
147 H. Ma, J. Cui, J. Chen and J. Hao, *Chem.–Eur. J.*, 2011, **17**, 655–660.
148 J. Wang, C.-F. Wang, H.-X. Shen and S. Chen, *Chem. Commun.*, 2010, **46**, 7376–7378.
149 X. Jiang, X. Zhou, Y. Zhang, T. Zhang, Z. Guo and N. Gu, *Langmuir*, 2009, **26**, 2477–2483.
150 J. H. Kim, M. Seo and S. Y. Kim, *Adv. Mater.*, 2009, **21**, 4130–4133.
151 S. S. Babu, S. Mahesh, K. K. Kartha and A. Ajayaghosh, *Chem.–Asian J.*, 2009, **4**, 824–829.
152 M. Zhang, S. Sun, X. Yu, X. Cao, Y. Zou and T. Yi, *Chem. Commun.*, 2010, **46**, 3553–3555.
153 L. A. Connal and G. G. Qiao, *Adv. Mater.*, 2006, **18**, 3024–3028.
154 L. A. Connal, R. Vestberg, C. J. Hawker and G. G. Qiao, *Adv. Funct. Mater.*, 2008, **18**, 3315–3322.
155 L. A. Connal and G. G. Qiao, *Soft Matter*, 2007, **3**, 837–839.
156 L. A. Connal, R. Vestberg, P. A. Gurr, C. J. Hawker and G. G. Qiao, *Langmuir*, 2008, **24**, 556–562.
157 L. Li, Y. Zhong, J. Gong, J. Li, C. Chen, B. Zeng and Z. Ma, *Soft Matter*, 2011, **7**, 546–552.
158 C. Greiser, S. Ebert and W. A. Goedel, *Langmuir*, 2008, **24**, 617–620.
159 T. Nishikawa, R. Ookura, J. Nishida, K. Arai, J. Hayashi, N. Kurono, T. Sawadaishi, M. Hara and M. Shimomura, *Langmuir*, 2002, **18**, 5734–5740.
160 C. X. Cheng, Y. Tian, Y. Q. Shi, R. P. Tang and F. Xi, *Langmuir*, 2005, **21**, 6576–6581.
161 H. Ma, J. Cui, A. Song and J. Hao, *Chem. Commun.*, 2011, **47**, 1154–1156.
162 S. R. S. Ting, E. H. Min, P. Escalé, M. Save, L. Billon and M. H. Stenzel, *Macromolecules*, 2009, **42**, 9422–9434.
163 L. A. Connal, G. V. Franks and G. G. Qiao, *Langmuir*, 2010, **26**, 10397–10400.
164 J. Nishida, K. Nishikawa, S. I. Nishimura, S. Wada, T. Karino, T. Nishikawa, K. Ijiro and M. Shimomura, *Polym. J.*, 2002, **34**, 166–174.
165 K. H. Wong, T. P. Davis, C. Barner-Kowollik and M. H. Stenzel, *Polymer*, 2007, **48**, 4950–4965.
166 F. Galeotti, V. Calabrese, M. Cavazzini, S. Quici, C. Poleunis, S. Yunus and A. Bolognesi, *Chem. Mater.*, 2010, **22**, 2764–2769.
167 E. H. Min, K. H. Wong and M. H. Stenzel, *Adv. Mater.*, 2008, **20**, 3550–3556.
168 M. Hernández-Guerrero, E. Min, C. Barner-Kowollik, A. H. E. Müller and M. H. Stenzel, *J. Mater. Chem.*, 2008, **18**, 4718–4730.
169 E. H. Min, S. R. S. Ting, L. Billon and M. H. Stenzel, *J. Polym. Sci., Part A: Polym. Chem.*, 2010, **48**, 3440–3455.

170 B.-B. Ke, L.-S. Wan and Z.-K. Xu, *Langmuir*, 2010, **26**, 8946–8952.
171 D. Nyström, E. Malmström, A. Hult, I. Blakey, C. Boyer, T. P. Davis and M. R. Whittaker, *Langmuir*, 2010, **26**, 12748–12754.
172 Y. Zhang and C. Wang, *Adv. Mater.*, 2007, **19**, 913–916.
173 H. Yabu, M. Tanaka, K. Ijiro and M. Shimomura, *Langmuir*, 2003, **19**, 6297–6300.
174 A. Bolognesi, F. Galeotti, J. Moreau, U. Giovanella, W. Porzio, G. Scavia and F. Bertini, *J. Mater. Chem.*, 2010, **20**, 1483–1488.
175 B. Erdogan, L. Song, J. N. Wilson, J. O. Park, M. Srinivasarao and U. H. F. Bunz, *J. Am. Chem. Soc.*, 2004, **126**, 3678–3679.
176 H. Yabu, M. Kojima, M. Tsubouchi, S. Onoue, M. Sugitani and M. Shimomura, *Colloids Surf., A*, 2006, **284–285**, 254–256.
177 A. S. Karikari, S. R. Williams, C. L. Heisey, A. M. Rawlett and T. E. Long, *Langmuir*, 2006, **22**, 9687–9693.
178 O. Karthaus, Y. Hashimoto, K. Kon and Y. Tsuriga, *Macromol. Rapid Commun.*, 2007, **28**, 962–965.
179 T. Kabuto, Y. Hashimoto and O. Karthaus, *Adv. Funct. Mater.*, 2007, **17**, 3569–3573.
180 L. Li, Y. Zhong, J. Li, C. Chen, A. Zhang, J. Xu and Z. Ma, *J. Mater. Chem.*, 2009, **19**, 7222–7227.
181 L. Li, C. Chen, J. Li, A. Zhang, X. Liu, B. Xu, S. Gao, G. Jin and Z. Ma, *J. Mater. Chem.*, 2009, **19**, 2789–2796.
182 L. Li, C. Chen, A. Zhang, X. Liu, K. Cui, J. Huang, Z. Ma and Z. Han, *J. Colloid Interface Sci.*, 2009, **331**, 446–452.
183 K. H. Wong, M. H. Stenzel, S. Duvall and F. Ladouceur, *Chem. Mater.*, 2010, **22**, 1878–1891.
184 M. Kojima, T. Nakanishi, Y. Hirai, H. Yabu and M. Shimomura, *Chem. Commun.*, 2010, **46**, 3970–3972.
185 T. Nakanishi, Y. Hirai, M. Kojima, H. Yabu and M. Shimomura, *J. Mater. Chem.*, 2010, **20**, 6741–6745.
186 H. Ejima, T. Iwata and N. Yoshie, *Macromolecules*, 2008, **41**, 9846–9848.
187 B. C. Englert, S. Scholz, P. J. Leech, M. Srinivasarao and U. H. F. Bunz, *Chem.–Eur. J.*, 2005, **11**, 995–1000.
188 K. Zhang, L. Zhang and Y. Chen, *Macromol. Rapid Commun.*, 2007, **28**, 2024–2028.
189 H. Zhao, Y. Shen, S. Zhang and H. Zhang, *Langmuir*, 2009, **25**, 11032–11037.
190 K. Kon, C. N. Brauer, K. Hidaka, H.-G. Löhmannsröben and O. Karthaus, *Langmuir*, 2010, **26**, 12173–12176.
191 L. Li, Y. Zhong, C. Ma, J. Li, C. Chen, A. Zhang, D. Tang, S. Xie and Z. Ma, *Chem. Mater.*, 2009, **21**, 4977–4983.
192 C.-Y. Ma, Y.-W. Zhong, J. Li, C.-K. Chen, J.-L. Gong, S.-Y. Xie, L. Li and Z. Ma, *Chem. Mater.*, 2010, **22**, 2367–2374.
193 B. de Boer, U. Stalmach, H. Nijland and G. Hadziioannou, *Adv. Mater.*, 2000, **12**, 1581–1583.
194 Y. Lu, Y. Ren, L. Wang, X. Wang and C. Li, *Polymer*, 2009, **50**, 2035–2039.
195 N. E. Zander, J. A. Orlicki, A. S. Karikari, T. E. Long and A. M. Rawlett, *Chem. Mater.*, 2007, **19**, 6145–6149.
196 W. Sun, L. Shen, J. Wang, K. Fu and J. Ji, *Langmuir*, 2010, **26**, 14236–14240.
197 H. Yabu, M. Takebayashi, M. Tanaka and M. Shimomura, *Langmuir*, 2005, **21**, 3235–3237.
198 D. Ishii, H. Yabu and M. Shimomura, *Chem. Mater.*, 2009, **21**, 1799–1801.
199 Y. Hirai, H. Yabu, Y. Matsuo, K. Ijiro and M. Shimomura, *Chem. Commun.*, 2010, **46**, 2298–2300.
200 T. Nishikawa, M. Nonomura, K. Arai, J. Hayashi, T. Sawadaishi, Y. Nishiura, M. Hara and M. Shimomura, *Langmuir*, 2003, **19**, 6193–6201.
201 H. Yabu, R. Jia, Y. Matsuo, K. Ijiro, S. Yamamoto, F. Nishino, T. Takaki, M. Kuwahara and M. Shimomura, *Adv. Mater.*, 2008, **20**, 4200–4204.
202 R. D. Deegan, O. Bakajin, T. F. Dupont, G. Huber, S. R. Nagel and T. A. Witten, *Nature*, 1997, **389**, 827–829.
203 R. D. Deegan, O. Bakajin, T. F. Dupont, G. Huber, S. R. Nagel and T. A. Witten, *Phys. Rev. E*, 2000, **62**, 756–765.
204 S. Maenosono, C. D. Dushkin, S. Saita and Y. Yamaguchi, *Langmuir*, 1999, **15**, 957–965.
205 F. I. Li, S. M. Thaler, P. H. Leo and J. A. Barnard, *J. Phys. Chem. B*, 2006, **110**, 25838–25843.
206 T. Kajiya, D. Kaneko and M. Doi, *Langmuir*, 2008, **24**, 12369–12374.
207 T. T. Nellimoottil, P. N. Rao, S. S. Ghosh and A. Chattopadhyay, *Langmuir*, 2007, **23**, 8655–8658.
208 K. F. Baughman, R. M. Maier, T. A. Norris, B. M. Beam, A. Mudalige, J. E. Pemberton and J. Curry, *Langmuir*, 2010, **26**, 7293–7298.
209 I. I. Smalyukh, O. V. Zribi, J. C. Butler, O. D. Lavrentovich and G. C. L. Wong, *Phys. Rev. Lett.*, 2006, **96**, 177801.
210 R. D. Deegan, *Phys. Rev. E*, 2000, **61**, 475–485.
211 A. P. Sommer and N. Rozlosnik, *Cryst. Growth Des.*, 2005, **5**, 551–557.
212 F. F. Shao, A. Neild and T. W. Ng, *J. Appl. Phys.*, 2010, **108**, 034512.
213 C. H. Chon, S. Paik, J. B. Tipton Jr. and K. D. Kihm, *Langmuir*, 2007, **23**, 2953–2960.
214 A. S. Sangani, C. Lu, K. Su and J. A. Schwarz, *Phys. Rev. E*, 2009, **80**, 11603.
215 H. Hu and R. G. Larson, *Langmuir*, 2005, **21**, 3972–3980.
216 H. Hu and R. G. Larson, *J. Phys. Chem. B*, 2006, **110**, 7090–7094.
217 J. Park and J. Moon, *Langmuir*, 2006, **22**, 3506–3513.
218 T. Kajiya, C. Monteux, T. Narita, F. Lequeux and M. Doi, *Langmuir*, 2009, **25**, 6934–6939.
219 T. Kajiya, W. Kobayashi, T. Okuzono and M. Doi, *J. Phys. Chem. B*, 2009, **113**, 15460–15466.
220 V. X. Nguyen and K. J. Stebe, *Phys. Rev. Lett.*, 2002, **88**, 164501.
221 V. N. Truskett and K. J. Stebe, *Langmuir*, 2003, **19**, 8271–8279.
222 H. Ma, R. Dong, J. D. Van Horn and J. Hao, *Chem. Commun.*, 2011, **47**, 2047–2049.
223 T. S. Wong, A. P. H. Huang and C. M. Ho, *Langmuir*, 2009, **25**, 6599–6603.
224 X. Shen, C. M. Ho and T. S. Wong, *J. Phys. Chem. B*, 2010, **114**, 5269–5274.
225 V. Dugas, J. Broutin and E. Souteyrand, *Langmuir*, 2005, **21**, 9130–9136.
226 J. A. Lim, W. H. Lee, H. S. Lee, J. H. Lee, Y. D. Park and K. Cho, *Adv. Funct. Mater.*, 2008, **18**, 229–234.
227 A. P. Sommer and R. P. Franke, *Nano Lett.*, 2003, **3**, 573–575.
228 F. I. Li, P. H. Leo and J. A. Barnard, *J. Phys. Chem. B*, 2008, **112**, 16497–16504.
229 S. Magdassi, M. Grouchko, D. Toker, A. Kamyshny, I. Balberg and O. Millo, *Langmuir*, 2005, **21**, 10264–10267.
230 M. Layani, M. Gruchko, O. Milo, I. Balberg, D. Azulay and S. Magdassi, *ACS Nano*, 2009, **3**, 3537–3542.
231 S. Choi, S. Stassi, A. P. Pisano and T. I. Zohdi, *Langmuir*, 2010, **26**, 11690–11698.
232 E. Adachi, A. S. Dimitrov and K. Nagayama, *Langmuir*, 1995, **11**, 1057–1060.
233 L. Shmuylovich, A. Q. Shen and H. A. Stone, *Langmuir*, 2002, **18**, 3441–3445.
234 S. Maheshwari, L. Zhang, Y. Zhu and H. C. Chang, *Phys. Rev. Lett.*, 2008, **100**, 44503.
235 L. Zhang, S. Maheshwari, H. C. Chang and Y. Zhu, *Langmuir*, 2008, **24**, 3911–3917.
236 M. A. Ray, H. Kim and L. Jia, *Langmuir*, 2005, **21**, 4786–4789.
237 Z. Lin and S. Granick, *J. Am. Chem. Soc.*, 2005, **127**, 2816–2817.
238 S. W. Hong, J. Xu, J. Xia, Z. Lin, F. Qiu and Y. Yang, *Chem. Mater.*, 2005, **17**, 6223–6226.
239 J. Xu, J. Xia, S. W. Hong, Z. Lin, F. Qiu and Y. Yang, *Phys. Rev. Lett.*, 2006, **96**, 066104.
240 J. Xu, J. Xia and Z. Lin, *Angew. Chem., Int. Ed.*, 2007, **46**, 1860–1863.
241 S. W. Hong, J. Xia and Z. Lin, *Adv. Mater.*, 2007, **19**, 1413–1417.
242 S. W. Hong, J. Wang and Z. Lin, *Angew. Chem., Int. Ed.*, 2009, **48**, 8356–8360.
243 S. W. Hong, M. Byun and Z. Lin, *Angew. Chem., Int. Ed.*, 2009, **48**, 512–516.
244 M. Byun, N. B. Bowden and Z. Lin, *Nano Lett.*, 2010, **10**, 3111–3117.
245 S. W. Hong, S. Giri, V. S. Y. Lin and Z. Lin, *Chem. Mater.*, 2006, **18**, 5164–5166.
246 S. W. Hong, J. Xu and Z. Lin, *Nano Lett.*, 2006, **6**, 2949–2954.
247 S. W. Hong, W. Jeong, H. Ko, M. R. Kessler, V. V. Tsukruk and Z. Lin, *Adv. Funct. Mater.*, 2008, **18**, 2114–2122.